Tribology International 69 (2014) 128–140

Contents lists available at ScienceDirect

Tribology International

journal homepage: www.elsevier.com/locate/triboint

Development of an innovative wheel–rail contact model for the analysis of degraded adhesion in railway systems

B. Allotta, E. Meli *, A. Ridolfi, A. Rindi

Department of Industrial Engineering, University of Florence, via S. Marta n. 3, 50139 Firenze, Italy

ARTICLE INFO

Article history:
Received 16 May 2013
Received in revised form
11 September 2013
Accepted 15 September 2013
Available online 25 September 2013

Keywords:
Wheel–rail adhesion
Degraded adhesion
Adhesion recovery

ABSTRACT

A detailed description of adhesion is crucial in tribology, vehicle dynamics and railway systems, both theoretically and practically. However, an accurate adhesion model is quite hard to develop because of the complex and non-linear behaviour of the adhesion coefficient and the external unknown contaminants which are present between the contact surfaces. The problem becomes even more complicated when degraded adhesion and large sliding between the contact bodies (for instance wheel and rail) occur.

In this paper the authors describe an innovative adhesion model aimed at increasing the accuracy in reproducing degraded adhesion conditions in vehicle dynamics and railway systems; the new approach turns out to be quite suitable also for multibody applications (fundamental in this research topic). The model studied in the work considers some of the main phenomena behind the degraded adhesion: the large sliding at the contact interface, the high energy dissipation, the consequent cleaning effect on the contact surfaces and, finally, the adhesion recovery due to the external unknown contaminant removal.

The new adhesion model has been validated through experimental data provided by Trenitalia S.p.A. and coming from on-track tests carried out in Velim (Czech Republic) on a straight railway track characterised by degraded adhesion conditions. The tests have been performed with the railway vehicle UIC-Z1 equipped with a fully-working Wheel Slide Protection (WSP) system.

The validation showed the good performances of the adhesion model both in terms of accuracy and in terms of numerical efficiency; high computational performances are required to implement the developed model directly online within more general and complex multibody models (e.g. in Matlab-Simulink and Simpack environments). In conclusion, the adhesion model highlighted the capability of well reproducing the complex phenomena behind the degraded adhesion.

1. Introduction

An accurate adhesion modelling plays a fundamental role in tribology, vehicle dynamics and railway systems as it deeply affects the dynamics, the wear processes and the safety of the considered systems, both from a theoretical and a practical point of view. The adhesion coefficient is characterised by a highly complex and non-linear behaviour, especially in presence of degraded adhesion and large sliding between the contact surfaces due to external unknown contaminants. For this reason the complete understanding and the modelling of the degraded adhesion are today important open problems.

With regard to the state-of-the-art of the discipline and, in particular, the railway applications where the multibody approaches are prevalent, the models usually employed in the research activities to describe the contact and adhesion phenomena do not take into account the complex degraded adhesion behaviour and the effect of the presence of the external contaminants.

This kind of models necessarily represents a trade-off between accuracy and numerical efficiency and consists of three fundamental logical steps: the detection of the contact point positions [2,7,8,3–5], the calculation of the normal contact forces (based on the improvements of the Hertz theory [9,3,4,5]) and the evaluation of the tangential contact forces (mainly based on the Kalker theory [9] and the Polach one [1,6]).

Nevertheless, in the last decades, many noteworthy studies and analyses have been carried out to investigate the role of the so-called third body between the surfaces of the contact bodies, e.g. wheels and rails. Important analyses have been performed on laboratory test rigs by considering natural contaminants (water, sand, etc.) [15,18,22] and artificial friction modifiers [13,16,21,14,20]. The performances of the contaminants have been

* Corresponding author. Tel.: +39 0 554796286; fax: +39 0 554796342.
E-mail addresses: enrico.meli@unifi.it, meli@mapp1.de.unifi.it (E. Meli).

0301-679X/$ - see front matter © 2013 Elsevier Ltd. All rights reserved.
http://dx.doi.org/10.1016/j.triboint.2013.09.013

compared to each other in [19]. Fundamental studies have been carried out through on-track railway tests too by taking into account natural contaminants [12] and artificial friction modifiers [10,11]. In that case, a comparison between the contaminants can be found in [17].

Also the main phenomena behind the degraded adhesion have been more and more accurately studied, starting from the presence of the large sliding at the contact interface [23,24], the high energy dissipation [25,26], the consequent cleaning effect on the contact surfaces and, finally, the adhesion recovery due to the removal of the external unknown contaminants [25,26]. The authors previously investigated this important topics on scaled railway test rigs [27], on full scale ones [29,41] and through on-track railway tests [28,30].

The model described by the authors in this paper aims to increase the accuracy in reproducing degraded adhesion conditions in vehicle dynamics and railway systems. Furthermore the new approach turns out to be suitable for multibody applications (for instance in Matlab-Simulink and Simpack environments [31,32]), which are very important in the considered research field. High computational performances are needed so that the new adhesion model could be directly implemented online in more general multibody models.

The new model focuses on the main phenomena characterising the degraded adhesion and, according to the recent trends of the state-of-the-art, pays particular attention to the energy dissipation at the contact interface, the consequent cleaning effect and the resulting adhesion recovery due to the removal of the external unknown contaminants. Moreover, the simplicity of the followed approach permits the minimisation of the number of model physical parameters that are very difficult to be experimentally measured. This interesting feature is fundamental because most of the physical characteristics of the contaminants are totally unknown in practice.

The new adhesion model has been validated through experimental data provided by Trenitalia S.p.A. and coming from on-track tests carried out in Velim (Czech Republic) on a straight railway track characterised by degraded adhesion conditions. The tests have been performed with the railway vehicle UIC-Z1 equipped with a fully-working Wheel Slide Protection (WSP) system [33–35].

The structure of the paper is as follows: in Section 2 the new degraded adhesion model for railway systems will be described in detail, while in Section 3 the experimental data will be introduced; the validation of the model will be discussed in Section 4 and in Section 5 a possible implementation of the adhesion model in the multibody model of a railway vehicle will be illustrated; finally, conclusions and further developments will be proposed in Section 6.

2. The degraded adhesion model

In this section the new degraded adhesion model will be described in detail. As discussed in the introduction, the model presented by the authors aims to increase the accuracy of the existing adhesion models when low adhesion conditions are present on the railway line. In particular degraded adhesion conditions are characterised by a large sliding between wheel and rail (caused for instance by the presence of the external contaminants between the contact surfaces and traction and braking manoeuvres) and, consequently, by a high energy dissipation occurring at the contact interface due to the work of the friction forces. To describe the degraded adhesion behaviour, the presented work considers the presence of the third body between wheel and rail (oxides, soil, wear debris, water, etc.). The work of the friction forces provokes a cleaning effect on the contact surfaces and, subsequently, an adhesion recovery due to the removal of the external contaminants. This cleaning effect may also bring back the adhesion coefficient to values typical of dry contact conditions.

This issue is fundamental in the railway field because, in practice, a layer of the external contaminants is always present on the rails and its physical characteristics are usually totally unknown. Furthermore, there may be some differences in terms of adhesion coefficient between the wheels of the same train; in particular the cleaning effect due to the action of the first wheels guarantees better adhesion conditions to the following wheels. At this initial phase of the research activity, such differences have not been taken into account.

The main inputs of the degraded adhesion model are the wheel velocity v_w, the wheel angular velocity ω_w, the normal force at the contact interface N_c and the contact point position P_c. The model also requires the knowledge of some wheel–rail and contact parameters that will be introduced along this section. The outputs are the adhesion coefficient f and the tangential contact force T_c (see Fig. 1).

During the initial phase of the model development, the detailed analysis of only the degraded adhesion model (separated from the dynamical vehicle model that will be considered in Section 5) will be performed: particularly in Section 2 the new adhesion model will be described, in Section 3 the processing of the experimental data will be discussed and in Section 4 the tuning and the validation of the model will be analysed.

Therefore, during this phase, the degraded adhesion model is static: more in detail, it can be considered as a static function (a black box) characterised by inputs (in this case experimental) and outputs (to be compared with the correspondent experimental quantities to evaluate the model accuracy). Moreover, at this step,

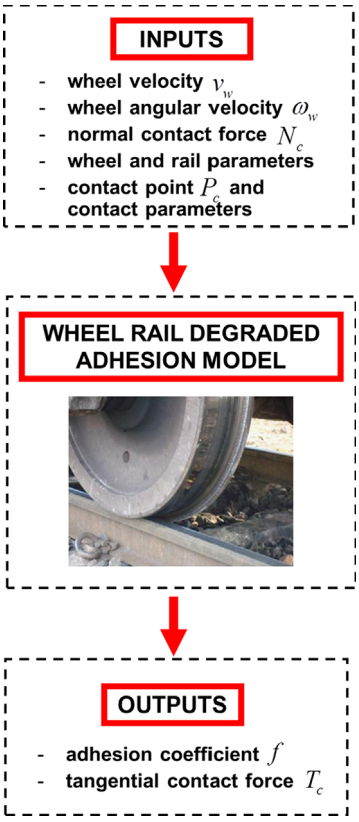

Fig. 1. Inputs and outputs of the degraded adhesion model.

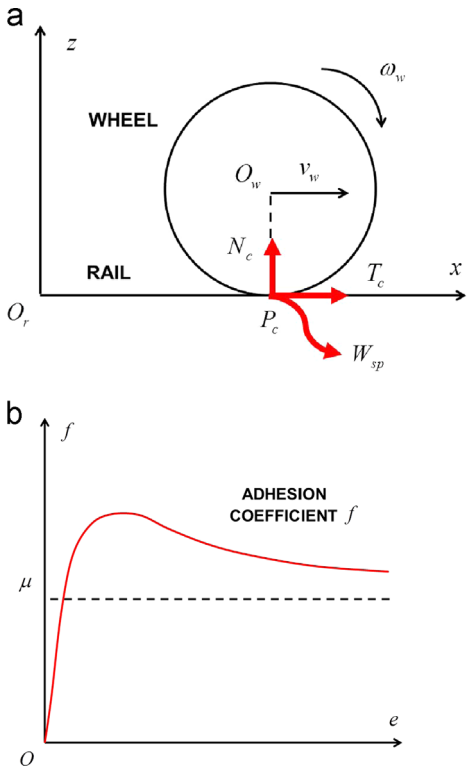

Fig. 2. One-dimensional (1D) scheme of the degraded adhesion model (a); standard behaviour of the adhesion coefficient f (b).

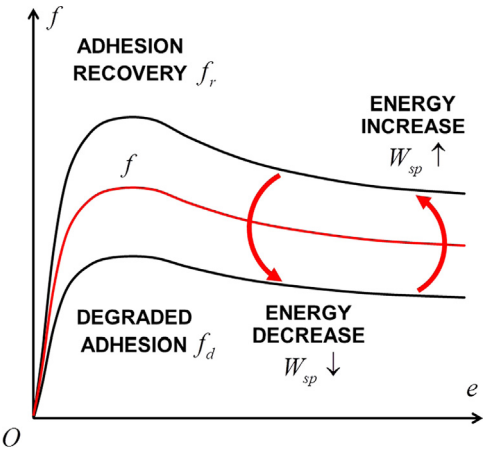

Fig. 3. The adhesion coefficient f and the specific dissipated energy W_{sp} under degraded adhesion conditions.

the dynamics of the wheel is considered, for simplicity, one-dimensional (1D).

The wheel one-dimensional (1D) model is briefly illustrated in Fig. 2a, where W_{sp} is the specific energy dissipated at the contact (see Eq. (1)).

If the adhesion recovery due to the cleaning effect caused by the dissipated energy W_{sp} and the work of friction forces is not considered, the adhesion coefficient f is characterised by the typical behaviour (as a function of the creepage e defined in Eq. (1)) predicted by the Kalker and Polach theories [1,6,9] and in agreement with the experimental results (linearly increasing for small creepage and asymptotically decreasing for large creepage); see for instance Fig. 2b.

Otherwise, if the adhesion recovery is considered, the adhesion coefficient f is characterised by the following qualitative behaviour (see Fig. 3):

1) if the dissipated energy W_{sp} is small (for instance due to a small creepage e), the cleaning effect of the friction forces is almost absent and the contaminant thickness h does not change; consequently, the adhesion coefficient f remains equal to its minimum value f_d under degraded adhesion conditions;
2) as the dissipated energy W_{sp} (due to a larger creepage e), the cleaning effect becomes more important, the external contaminant is destroyed by the work of the friction forces (the contaminant thickness h decreases) and, consequently, the adhesion coefficient f increases;
3) when the dissipated energy W_{sp} increases up to completely destroy the contaminant between wheel and rail and the contaminant thickness h is equal to zero (due to a very large creepage e), the adhesion coefficient increases up to reach its maximum value f_r, approximately equal to the value under dry adhesion conditions. The adhesion recovery due to the cleaning effect and the removal of external contaminants is now completed;
4) at the same time if the dissipated energy W_{sp} and the work of the friction forces begin to decrease (due to a lower creepage e), the reverse process occurs: a less effective cleaning effect is present, the contaminant thickness h increases and, consequently, the adhesions coefficient f decreases towards its minimum value f_d.

The degraded adhesion model presented in this section aims at approximately describing the behaviour of the adhesion coefficient f previously analysed.

From a theoretical point of view, firstly the dissipated energy W_{sp} should be connected to the quantity of removed contaminants and thus to the contaminant thickness h. Secondly, the contaminant thickness h should be linked to the adhesion coefficient f: as the thickness h decreases from its initial value (absence of cleaning effect) to zero (complete removal of the third body), the adhesion coefficient f varies from the minimum value f_d (degraded adhesion) to the maximum value f_r (complete adhesion recovery).

However, this way the adhesion model would be much more complicated from an analytical viewpoint and require many numerical parameters quite difficult to be experimentally measured and tuned. For this reason, it is advantageous to directly connect (both analytically and experimentally) the dissipated energy W_{sp} to the adhesion coefficient f. This approach turns out to be analytically simpler than the previous one and easier to be experimentally tuned; moreover it represents a good trade-off between accuracy and numerical efficiency.

To reach this goal, firstly the adhesion coefficient f and the specific dissipated energy W_{sp} have to be defined:

$$W_{sp} = T_c e = f N_c e \quad f = \frac{T_c}{N_c} \tag{1}$$

where the creepage e can be calculated as:

$$e = \frac{s}{v_w} = \frac{v_w - r\omega_w}{v_w}, \tag{2}$$

s is the sliding and r is the wheel radius. This way the specific dissipated energy W_{sp} can also be interpreted as the energy dissipated at the contact per unit of distance covered by the railway vehicle.

To reproduce the qualitative trend previously described and allow the adhesion coefficient to vary between the extreme values f_d and f_r, the following expression for f is proposed:

$$f = [1 - \lambda(W_{sp})] f_d + \lambda(W_{sp}) f_r \tag{3}$$

where $\lambda(W_{sp})$ is an unknown transition function between degraded adhesion and adhesion recovery. The function $\lambda(W_{sp})$ has to be positive and monotonously increasing; moreover the following boundary conditions are supposed to be verified: $\lambda(0)=0$ and $\lambda(+\infty)=1$.

This way the authors suppose the transition between degraded adhesion and adhesion recovery just depends on W_{sp}. This hypothesis is obviously just an approximation but, as it will be clearer in the next sections, it describes the complex adhesion behaviour. Initially, to catch the physical essence of the problem without introducing a large number of unmanageable and unmeasurable parameters, the authors have chosen the following simple expression for $\lambda(W_{sp})$:

$$\lambda(W_{sp}) = 1 - e^{-\tau W_{sp}} \tag{4}$$

where τ is now the only unknown parameter to be tuned on the base of the experimental data.

In this research activity the two main adhesion coefficients f_d and f_r (degraded adhesion and adhesion recovery) have been calculated according to Polach [1,6,9]:

$$\begin{aligned} f_d &= \frac{2\mu_d}{\pi}\left[\frac{k_{ad}\varepsilon_d}{1+(k_{ad}\varepsilon_d)^2} + \operatorname{arctg}(k_{sd}\varepsilon_d)\right] \\ f_r &= \frac{2\mu_r}{\pi}\left[\frac{k_{ar}\varepsilon_r}{1+(k_{ar}\varepsilon_r)^2} + \operatorname{arctg}(k_{sr}\varepsilon_r)\right] \end{aligned} \tag{5}$$

where

$$\varepsilon_d = \frac{1}{4}\frac{G\pi abc_{11}}{\mu_d N_c}e;\ \varepsilon_r = \frac{1}{4}\frac{G\pi abc_{11}}{\mu_r N_c}e \tag{6}$$

The quantities k_{ad}, k_{sd} and k_{ar}, k_{sr} are the Polach reduction factors (for degraded adhesion and adhesion recovery respectively) and μ_d, μ_r are the friction coefficient defined as follows:

$$\begin{aligned} \mu_d &= \left(\frac{\mu_{cd}}{A_d} - \mu_{cd}\right)e^{-\gamma_d S} + \mu_{cd} \\ \mu_r &= \left(\frac{\mu_{cr}}{A_r} - \mu_{cr}\right)e^{-\gamma_r S} + \mu_{cr} \end{aligned} \tag{7}$$

where μ_{cd}, μ_{cr} are the kinetic friction coefficients, A_d, A_r are the ratios between the kinetic friction coefficients and the static ones and γ_d, γ_r are the friction decrease rates. The Polach approach (see Eq. (5)) has been followed since it allows to describe the decrease of the adhesion coefficient with increasing creepage and to better fit the experimental data (see Figs. 2b and 3).

Finally, it has to be noticed that the semi-axes a and b of the contact patch (see Eq. (6)) depend only on the normal force N_c, the material properties (the Young modulus E, the shear modulus G and the Poisson coefficient σ) and the contact point position P_c on wheel and rail (through the curvatures of the contact surfaces in the contact point) while the contact shear stiffness C (N/m^3) is a function only of the semi-axes a and b and of the material properties [9]. In this simple 1D case Eq. (8) holds:

$$C = \frac{3Gc_{11}}{8a} \tag{8}$$

where $c_{11}=c_{11}(\sigma,a/b)$ is the Kalker coefficient [9]. At this first step of the model development, the contact point position P_c (single contact) is supposed to be known and nearly constant; in particular the wheel and rail profiles and the laying angle α_p are known, while the wheelset is supposed to be placed in its centred position (see the next sections for further details).

In the end, the desired values of the adhesion coefficient f and of the tangential contact force $T_c=fN_c$ can be evaluated by solving the algebraic Eq. (3) in which the explicit expression of $W_{sp}=fN_c e$ has been inserted (see Eq. (1)):

$$f = \mathfrak{I}(f, t) \tag{9}$$

where $\mathfrak{I}$ indicates the generic functional dependence. Due to the simplicity of the transition function $\lambda(W_{sp})$, the solution can be easily obtained through standard non-linear solvers [36]. From a computational point of view, the adhesion coefficient f_i can be computed at each integration time t_i by solving:

$$f_i = \mathfrak{I}(f_i, t_i). \tag{10}$$

3. Experimental results

3.1. The railway vehicle

The degraded adhesion model has been validated by means of experimental data [35], provided by Trenitalia S.p.A., coming from on-track tests performed in Velim (Czech Republic) with the coach UIC-Z1 (see Fig. 4). The considered vehicle is equipped with a fully-working Wheel Slide Protection (WSP) system. [33,34].

The coach consists of one carbody, two bogie frames, eight axleboxes, and four wheelsets. The vehicle has a two-stage suspension system: the primary suspension, including springs and dampers, connects the bogie frame to four axleboxes while the secondary suspension, including springs, dampers, lateral bump-stops, anti-roll bar and traction rod, connects the carbody to the bogie frames. In Table 1 the main properties of the railway vehicle are given.

3.2. The experimental tests

The experimental tests have been carried out on a straight track with the railway vehicle UIC-Z1 [35]. The wheel profile is the ORE S1002 (with a wheelset width d_w equal to 1.5 m and a wheel radius r equal to 0.445 m) while the rail profile is the UIC60 (with a gauge d_r equal to 1.435 m and a laying angle α_p equal to 1/20 rad). For the sake of simplicity, at this step of the model development, the wheelset is supposed to be placed in its centred position; this way the position of the contact points P_c (single contact) can be supposed to be known and nearly constant and the surface curvatures in the contact points, the semi-axes of the contact patch a, b and the contact shear stiffness C can be easily calculated [9]. In Table 2 the main wheel, rail and contact parameters are reported (see [1,6]).

Fig. 4. UIC-Z1 vehicle.

Table 1
Main characteristics of the railway vehicle.

Parameter	Units	Value
Total mass	kg	43000
Wheel arrangement	–	2–2
Bogie wheelbase	m	2.56
Bogie distance	m	19
Wheel diameter	m	0.89
Primary suspended masses own frequency	Hz	4.5
Secondary suspended masses own frequency	Hz	0.8

Table 2
Main wheel, rail and contact parameters.

Parameter	Units	Value
Young modulus E	Pa	2.1×10^{11}
Shear modulus G	Pa	8.0×10^{10}
Poisson coefficient σ	–	0.3
Polach reduction factor k_{ad}	–	0.3
Polach reduction factor k_{sd}	–	0.1
Polach reduction factor k_{ar}	–	1.0
Polach reduction factor k_{sr}	–	0.4
Kinetic friction coefficient μ_{cd}	–	0.06
Kinetic friction coefficient μ_{cr}	–	0.28
Friction ratio A_d	–	0.4
Friction ratio A_r	–	0.4
Friction decrease rate γ_d	s/m	0.2
Friction decrease rate γ_r	s/m	0.6

Table 3
Test initial velocities.

Parameter	Units	Value
Group A, I test	m/s	42.3
Group A, II test	m/s	40.4
Group A, III test	m/s	40.8
Group B, I test	m/s	40.8
Group B, II test	m/s	41.1
Group B, III test	m/s	41.8

Table 4
Relative errors e_1.between f_1^{sp}.and.f_1.

Parameters	Unit	A1	A2	A3	B1	B2	B3
e_1	(%)	3.8	4.3	3.3	5.1	4.8	4.5

The value of the kinetic friction coefficient under degraded adhesion conditions μ_{cd} (Table 2) depends on the test that has to be performed on the track.

The different degraded adhesion conditions have to be reproduced using a watery solution containing surface-active agents, e.g. a solution sprinkled by a specially provided nozzle directly on the wheel–rail interface on the first wheelset in the running direction (under a flow rate of 0.12 l/min to 0.19 l/min per tube through 8 mm diameter nozzles located along the longitudinal axis of the rail, a maximum of 70 mm from both the rail and the wheel).

The fluid used to reduce adhesion is an aqueous solution of a detergent with a fatty acid or surfactant base in a concentration below 15% and without mineral fillers. The detergent must be biodegradable, mix readily with water and be safe to dispose of in the track. The minimum concentration of the mixture must be such that for 100 l of water at least 1 l of agent is employed.

The surface-active agent concentration in the solution varies according to the type of test and the desired friction level. Changing coefficients of adhesion are produced by switching the spraying device on and off intermittently.

Such procedure is standard in the railway filed (see the current regulation in force UNI EN 15595 [40]) and allows to obtain quite precise and uniform adherence levels on the rails along the line. In particular, it allows to reach the desired value of the kinematic friction coefficient μ_{cd} (see Table 2) under degraded adhesion conditions (without adhesion recovery) and, consequently, of the correspondent adhesion coefficient f_d (see Eq. (5)).

On the other hand, the value of the kinetic friction coefficient under full adhesion recovery μ_{cs} (Table 2) corresponds to the classical kinetic friction coefficient under dry conditions.

During the experimental campaign six different braking tests have been performed. The six tests have been split into two groups (A and B): the first group has been used to tune the degraded adhesion model (in particular the unknown parameter τ, see Section 2, Eq. (4)) while the second one to properly validate the tuned model. The initial vehicle velocities corresponding to the considered tests are reported in Table 3.

For each test the following physical quantities have been measured (with a sample time Δt_s equal to 0.01 s):

1) the vehicle velocity v_v^{sp}. For the sake of simplicity all the wheel velocities v_{wj}^{sp} (j represents the $j-th$ wheel) are considered equal to v_v^{sp}. The acceleration of the vehicle a_v^{sp} and of the wheels a_{wj}^{sp} can be obtained by derivation and by properly filtering the numerical noise;
2) the angular velocities of all wheels ω_{wj}^{sp}. Also in this case the angular accelerations $\dot{\omega}_{wj}^{sp}$ can be calculated by derivation and by properly filtering;
3) the vertical loads N_{wj}^{sp} on the wheels. For the considered 1D model, the normal contact forces N_{cj}^{sp} can be evaluated starting from N_{wj}^{sp} by considering the weight of the wheels. At this first phase of the research activity, taking also into account that the experimental campaign has been performed on a straight flat line, the authors consider, as a first approximation, the simple static measure of the wheel weights (instead of a dynamic measure carried out during the experimental tests). Despite this initial approximation, the degraded adhesion model shows a good agreement with the experimental data;
4) the traction or braking torques C_{wj}^{sp} applied to the wheels.

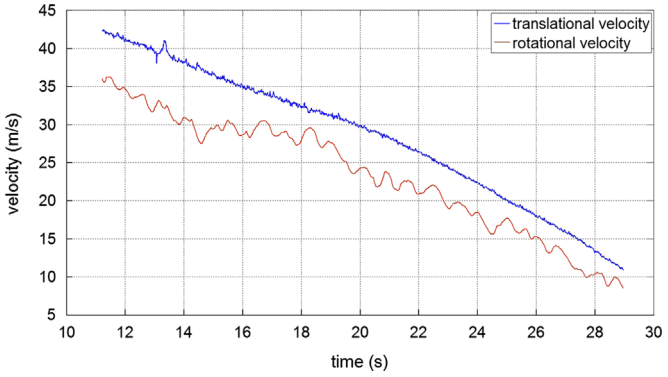

Fig. 5. Wheel translational and rotational velocities v_{w1}^{sp} and $r\omega_{w1}^{sp}$ for the I test of group A.

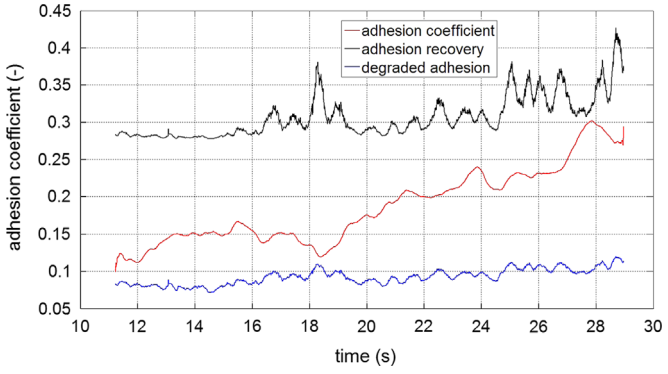

Fig. 6. Adhesion coefficient f_1^{sp} and its limit values f_{d1}^{sp}, f_{r1}^{sp} for the I test of group A.

By way of an example in Fig. 5 the wheel translational and rotational velocities v_{w1}^{sp} and $r\omega_{w1}^{sp}$ are reported for the I test of

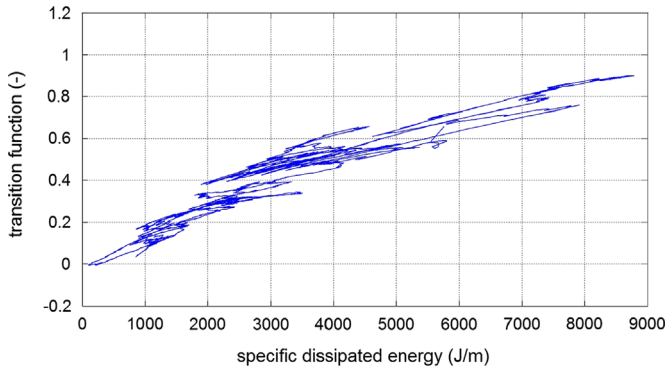

Fig. 7. Experimental transition function $\lambda_1^{sp}(W_{sp1}^{sp})$ for the I test of group A.

group A; both the WSP intervention and the adhesion recovery in the second part of the braking manoeuvre are clearly visible.

On the basis of the measured data (the experimental inputs of the degraded adhesion model), the experimental outputs of the model, e.g. the adhesion coefficient f_j^{sp}, the tangential contact force T_{cj}^{sp} and the transition function λ_j^{sp} have now to be computed for all tests. These experimental quantities are fundamental for the model validation described in the following section. Eq. (2) allows the calculation of s_j^{sp} and e_j^{sp} while T_{cj}^{sp} can be estimated through the rotational equilibrium of the wheel as to the origin O_w:

$$J_w\dot{\omega}_{wj}^{sp} = C_{wj}^{sp} - rT_{cj}^{sp} \tag{11}$$

where $J_w = 160\ \mathrm{kgm}^2$ is the wheel inertia. Subsequently Eq. (1) allows to calculate f_j^{sp} and the specific dissipation energy W_{spj}^{sp} while f_{dj}^{sp}, f_{rj}^{sp} can be computed directly through Eq. (5). Finally, from the knowledge of W_{spj}^{sp} and f_j^{sp}, f_{dj}^{sp}, f_{rj}^{sp}, the trend of the experimental transition function $\lambda_j^{sp}(W_{spj}^{sp})$ can be determined by means of Eq. (3). For instance in Fig. 6 the adhesion coefficient f_1^{sp} and its limit values f_{d1}^{sp}, f_{r1}^{sp} under degraded adhesion and adhesion recovery are illustrated always for the I test of group A (the adhesion recovery in the second part of the braking manoeuvre is clear). Fig. 7 shows the experimental trend of the transition function λ_1^{sp}.

The adhesion level arranged during the experimental campaign is in agreement both with the choice of the numerical parameters reported in Table 2 (in particular the kinematic friction factor μ_{cd} under degraded adhesion conditions) and with the measured experimental values of the adhesion coefficient f^{sp}: see, for instance, in Fig. 6 the time history of f_1^{sp} and especially of f_{d1}^{sp}, the adhesion coefficient under degraded adhesion conditions without any adhesion recovery (connected to μ_{cd} by Eq. (5)).

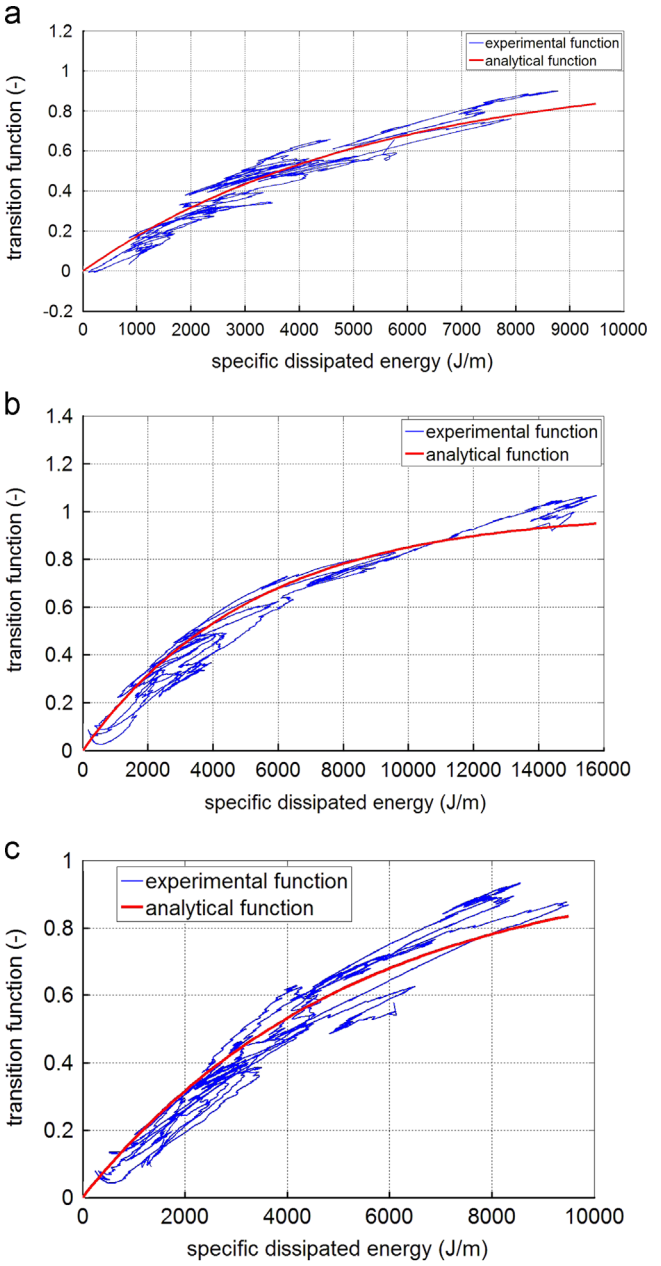

Fig. 8. Comparison between $\lambda(W_{sp})$ and $\lambda_1^{sp}(W_{sp1}^{sp})$ for the I (a), II (b) and III (c) test of group A.

4. Validation of the degraded adhesion model

4.1. Model tuning

During this phase of the research activity, the degraded adhesion model has been tuned on the basis of the three experimental braking tests of group A. In particular the attention focused on the transition function $\lambda(W_{sp})$ and on the τ parameter. Starting from the experimental transition functions $\lambda_j^{sp}(W_{spj}^{sp})$ corresponding to the three tests of group A, the parameter τ within $\lambda(W_{sp})$ has been tuned through a Non-linear Least Square Optimisation (NLSO) by minimising the following error function [37,36,31]:

$$g(\tau) = \sum_{k=1}^{3}\sum_{i=1}^{N_t}\sum_{j=1}^{N_w}[\lambda_{jk}^{sp}(W_{jk}^{sp}(t_i)) - \lambda(W_{jk}^{sp}(t_i))]^2 \tag{12}$$

where N_w is the wheel number and N_t is the measured sample number; this time, the index k indicates the k-th test of group A. In that case the optimisation process provided the optimum value $\tau = 1.9\times10^{-4}\mathrm{m/J}$. For instance, the comparisons between the optimised analytical transition function $\lambda(W_{sp})$ and the experimental transition function $\lambda_1^{sp}(W_{sp1}^{sp})$ are shown for the three tests of group A in Fig. 8.

Subsequently, always as for the tests of group A, the adhesion coefficient f_j has been calculated according to Section 2 by means of Eq. (10) starting from the knowledge of the experimental inputs v_{wj}^{sp}, ω_{wj}^{sp} and N_{cj}^{sp}; in this circumstance the optimised analytical transition function $\lambda(W_{sp})$ has been used. The behaviour of the calculated adhesion coefficient f_j has been compared with the experimental one f_j^{sp} (see Section 3). By way of example, in Fig. 9 the time histories of f_1 and f_1^{sp} are reported for all the tests of group A.

From a quantitative point of view, the relative errors $e_j = \|f_j^{sp} - f_j\|/\|f_j^{sp}\|$ between the experimental adhesion coefficient f_j^{sp} and the calculated one f_j have been considered. The values of e_1 for all the three tests of group A are summarised in Table 4.

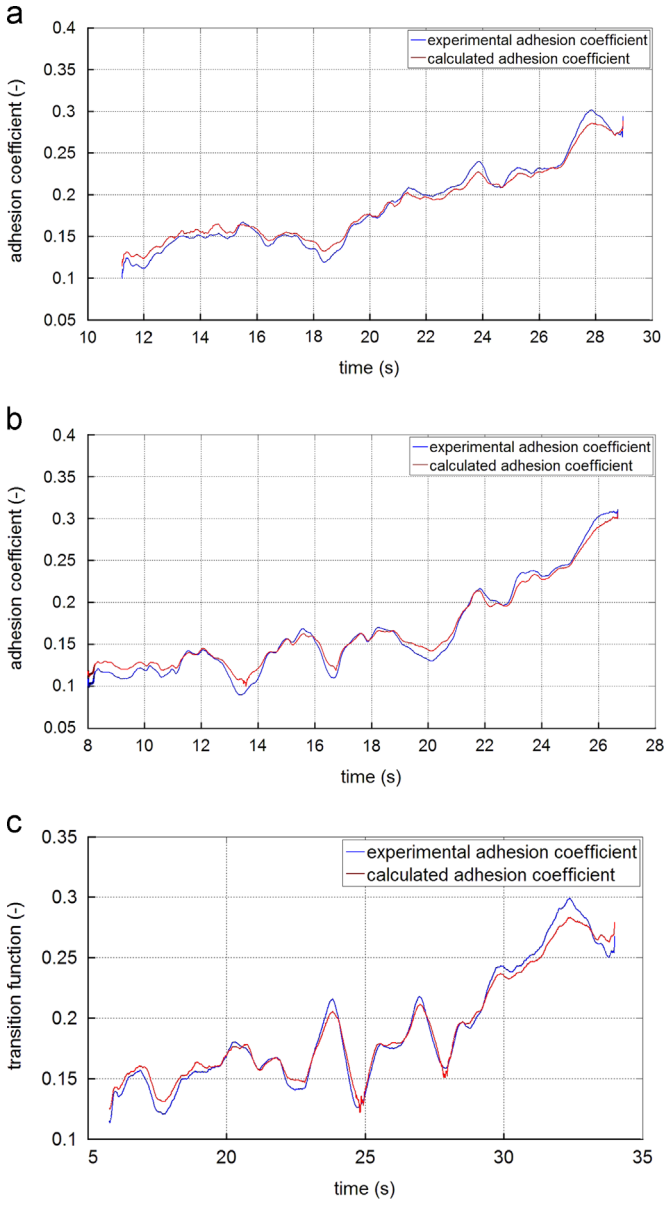

Fig. 9. Comparison between f_1 and f_1^{sp} for the I (a), II (b) and III (c) test of group A.

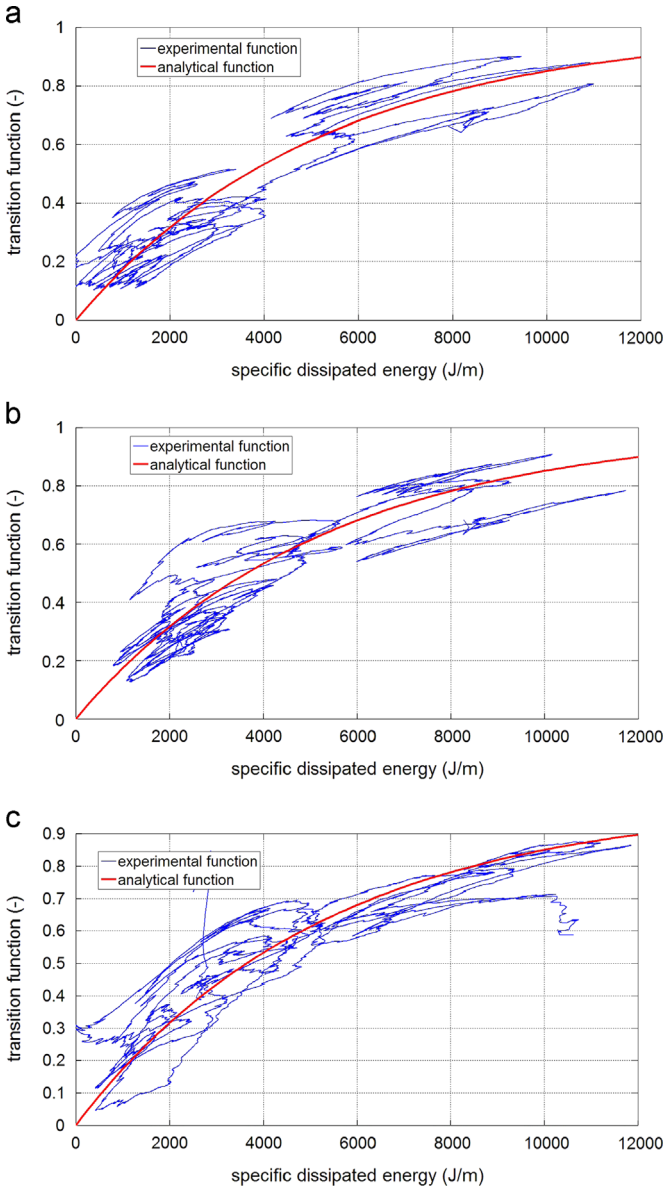

Fig. 10. Comparison between $\lambda(W_{sp})$ and $\lambda_1^{sp}(W_{sp1}^{sp})$ for the I (a), II (b) and III (c) test of group B.

The results of the tuning process highlight the good capability of the simple analytical transition function $\lambda(W_{sp})$ in reproducing the experimental trend of $\lambda_j^{sp}(W_{spj}^{sp})$ for all tests of group A. The good behaviour of the analytical transition function despite its simplicity (only one unknown parameter is involved) allows also a good matching of the experimental data in terms of the adhesion coefficient (see the trend of f_j and f_j^{sp} and the adhesion recovery in the second part of the braking manoeuvre).

4.2. Model validation

The real validation of the degraded adhesion model has been carried out by means of the three experimental braking tests of group B. Also in this case the attention focused first of all on the analytical transition function $\lambda(W_{sp})$ (the same tuned in paragraph IVA with $\tau = 1.9 \times 10^{-4}$m/J) and on its capability in matching the behaviour of the experimental transition functions $\lambda_j^{sp}(W_{spj}^{sp})$. The comparison between $\lambda(W_{sp})$ and $\lambda_1^{sp}(W_{sp1}^{sp})$ is illustrated in Fig. 10 for the tests of group B.

Similarly to paragraph IVA the adhesion coefficient f_j has been calculated for the tests of group B (see Section 2 and Eq. (10)) starting from the knowledge of the experimental inputs v_{wj}^{sp}, ω_{wj}^{sp} and N_{cj}^{sp}. Naturally the same analytical transition function $\lambda(W_{sp})$ optimised in paragraph IVA has been employed. The behaviour of the calculated adhesion coefficient f_j and the experimental one f_j^{sp} (see Section 3) have been compared again. For instance in Fig. 11 the time histories of f_1 and f_1^{sp} are reported for all the tests of group B.

Also in this case, the relative errors $e_j = \|f_j^{sp} - f_j\| / \|f_j^{sp}\|$ between the experimental adhesion coefficient f_j^{sp} and the calculated one f_j have been calculated. The values of e_1 for all the three tests of group B are summarised in Table 4.

The results of the model validation are encouraging and highlight the good matching between the analytical transition function $\lambda(W_{sp})$ (tuned in paragraph IVA on the base of the tests of group A) and the new experimental data $\lambda_j^{sp}(W_{spj}^{sp})$ concerning to the tests of group B. At the same time, also for group B, there is a good correspondence between the time histories of the calculated adhesion coefficient f_j and the ones of the experimental one f_j^{sp} (see the adhesion recovery in the second part of the braking

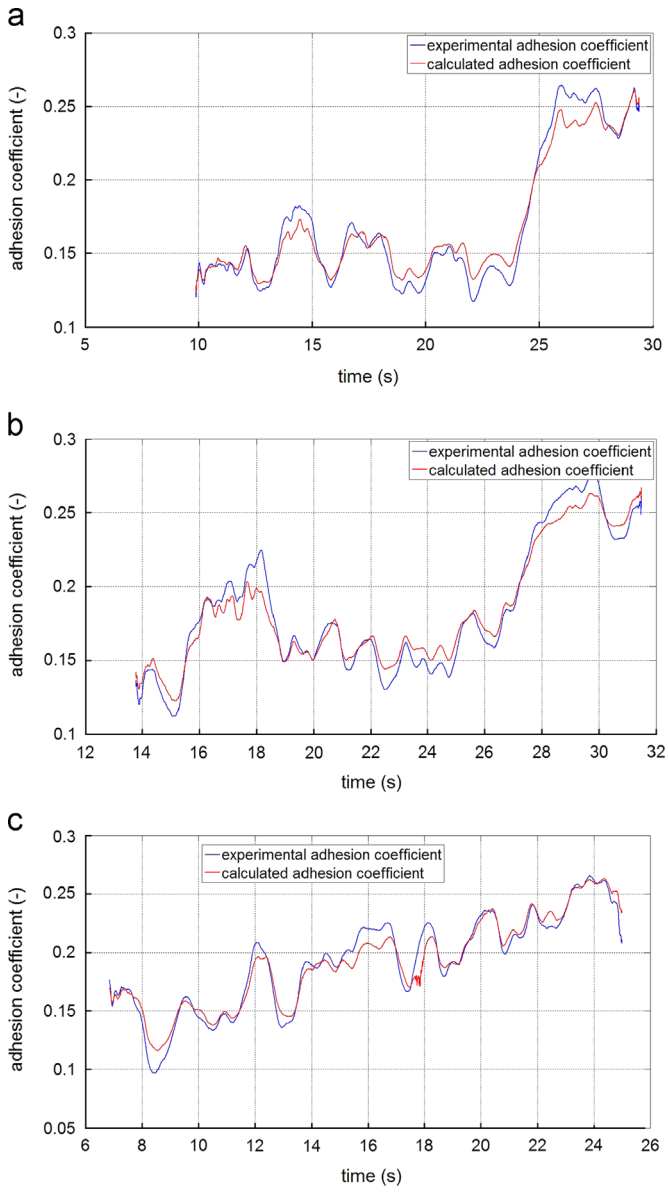

Fig. 11. Comparison between f_1 and f_1^{sp} for the I (a), II (b) and III (c) test of group B.

manoeuvre). The satisfying results obtained for the validation group B confirm the capability of the simple analytical transition function $\lambda(W_{sp})$ in approximating the complex and highly non-linear behaviour of the degraded adhesion.

Moreover, the new degraded adhesion model present two important advantages. Firstly, it just introduces one additional parameter (e.g. the τ rate), very easy to be experimentally tuned, without requiring the knowledge of further unknown physical properties of the contaminant. Secondly the model guarantees a very low computational load, making possible the online implementation of the procedure within more general multibody models built in dedicated environments [31,32].

5. Simulation of the vehicle dynamics

As a further validation of the degraded adhesion model, the new procedure has been inserted into a three-dimensional (3D) multibody model of the railway wagon UIC-Z1 to study the vehicle dynamics during the braking manoeuvre.

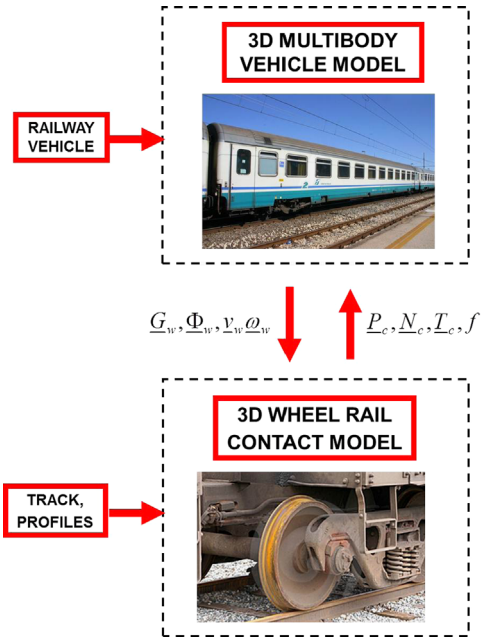

Fig. 12. Architecture of the multibody model.

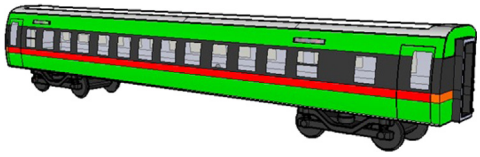

Fig. 13. Multibody vehicle model.

Table 5
Inertial properties of the rigid bodies.

Body	Mass (kg)	I_{xx}(kgm^2)	I_{yy} (kgm^2)	I_{zz}(kgm^2)
Carbody	29,000	76,400	1,494,400	1,467,160
Bogie	3000	2400	1900	4000
Wheelset	1300	800	160	800
Axlebox	200	3	12	12

The complete 3D model of the vehicle dynamics is equipped with a 3D, multi-contact wheel–rail contact model (see the bibliographic references [2,7,8]). In that case, the vehicle model and the adhesion model create a dynamic loop (unlike the initial case described in Section 2): the vehicle model calculates the inputs of the adhesion model while its outputs are passed back to the vehicle model to carry on the dynamical simulation.

5.1. The multibody model of the vehicle

The architecture of the multibody model is briefly reported in Fig. 12.

From a logical point of view, the multibody model consists of two different parts mutually interacting during the dynamical simulation: the model of the railway vehicle (whose geometrical and physical characteristics are known) and the contact model (multiple contact). At each time step the multibody vehicle model calculates the kinematic variables of each wheel (position $\underline{O}_w$, orientation $\underline{\Phi}_w$, velocity $\underline{v}_w$ and angular velocity $\underline{\omega}_w$) while the contact model, starting from the knowledge of these quantities, of the track geometry and of the wheel and rail profiles, evaluates the normal and tangential contact forces $\underline{N}_c$, $\underline{T}_c$ (applied to the wheel

in the contact point $\underline{P}_c$) and the adhesion coefficient f needed to carry on the simulation.

According to paragraph IIIA the multibody vehicle model (see Fig. 13) takes into account all degrees of freedom (DOF) of the system bodies (one carbody, two bogie frames, eight axleboxes, and four wheelsets). The inertial properties of the bodies are summarised in Table 5 [33].

Both the primary suspensions (springs and dampers) and the secondary suspensions (springs, dampers, lateral bump-stops, anti-roll bar and traction rod) have been modelled through 3D visco-elastic force elements able to describe all the main non-linearities of the system. In Table 6 the characteristics of the main linear elements of both the suspension stages are reported [33].

The wheel–rail contact model (multiple contact) includes three different steps: the detection of the contact points $\underline{P}_c$ (some innovative procedures have been recently developed by the authors in previous works [2,7,8]), the solution of the normal contact problem through the global Hertz theory [9] to evaluate the normal contact forces $\underline{N}_c$ and the solution of the tangential contact problem by means of the global Kalker–Polach theory [9,1,6] to compute the tangential contact forces $\underline{T}_c$ and the adhesion coefficient f (see the diagram in Fig. 14). Naturally both the railway track and the wheel and rail profiles are supposed to be known (see the Section 3.2).

Finally, also the Wheel Slide Protection (WSP) system of the railway wagon UIC-Z1 has been modelled to better investigate the vehicle behaviour during the braking phase under degraded

Table 6
Characteristics of the main linear elements (translational and rotational stiffness).

Element	Primary suspension	Secondary suspension	Anti-roll bar
Tr. Stiff. x (N/m)	8.44×10^5	1.24×10^5	0
Tr. Stiff. y (N/m)	8.44×10^5	1.24×10^5	0
Tr. Stiff. z (N/m)	7.9×10^5	3.4×10^5	0
Rot. Stiff. x (Nm/rad)	10,700	0	2.5×10^6
Rot. Stiff. y (Nm/rad)	10700	0	0
Rot. Stiff. z (Nm/rad)	0	0	0

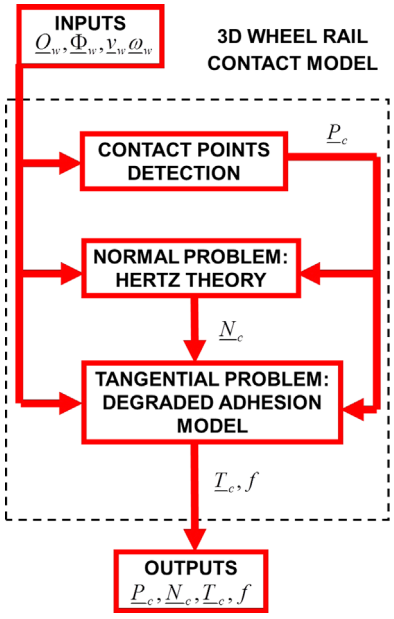

Fig. 14. Wheel–rail contact model.

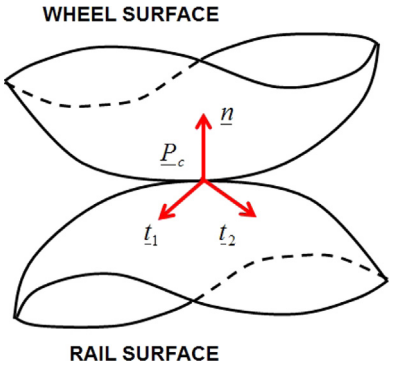

Fig. 15. Contact surfaces.

adhesion conditions [34,28]. The whole vehicle model has been implemented in the Matlab-Simulink environment [31].

Referring to Fig. 14, the new degraded adhesion model (see Section 2) can be easily inserted into the 3D contact model (multiple contact) of a generic 3D multibody system. In particular, for each contact point, starting from the wheel velocity $\underline{v}_w$, the wheel angular velocity $\underline{\omega}_w$, the contact point position $\underline{P}_c$ and the normal contact forces $\underline{N}_c$ (the inputs of the degraded adhesion model, directly provided by the multibody model, the contact point detection algorithm and the Hertz theory), the sliding $\underline{s}$ (together with its longitudinal and lateral components s_x, s_y) and the scalar normal contact force $\underline{N}_c$ can be determined:

$$\begin{aligned} &\underline{N}_c = N_c\underline{n} \quad N_c = \|\underline{N}_c\| \\ &\underline{s} = \underline{v}_w + \underline{\omega}_w \times (\underline{P}_c - \underline{O}_w) \\ &s = \|\underline{s}\| \quad s_x = \underline{s}\cdot\underline{t}_1 \quad s_y = \underline{s}\cdot\underline{t}_2 \end{aligned} \tag{13}$$

where $\underline{n}$, $\underline{t}_1$ and $\underline{t}_2$ are respectively the normal unit vector and the tangential unit vectors (in longitudinal and lateral direction) corresponding to the generic contact point $\underline{P}_c$ (see Fig. 15).

Subsequently the creepage $\underline{e}$ can be computed:

$$\begin{aligned} &\underline{e} = \frac{\underline{s}}{v_w} \quad v_w = \|\underline{v}_w\| \\ &e_x = \underline{e}\cdot\underline{t}_1 \quad e_y = \underline{e}\cdot\underline{t}_1 \end{aligned} \tag{14}$$

while, as regards the specific dissipated energy W_{sp}, the following relations hold:

$$\begin{aligned} &T_x = \underline{T}_c\cdot\underline{t}_1 = T_c\frac{e_x}{e} \quad T_y = \underline{T}_c\cdot\underline{t}_2 = T_c\frac{e_y}{e} \\ &e = \|\underline{e}\| \quad T_c = \|\underline{T}_c\| \\ &W_{sp} = \underline{T}_c\cdot\underline{e} = T_c e = fN_c e \end{aligned} \tag{15}$$

At this point, the scalar tangential contact force T_c and the adhesion coefficient f (the outputs of the degraded adhesion model) can be easily evaluated according to Section 2. In fact, since the contact point position $\underline{P}_c$ is provided by the contact point detection algorithm, the contact surface curvatures and consequently the contact patch semi-axes a, b and the contact shear stiffness C are known [9]. In this more general 3D case, C has the following expression:

$$C = \frac{3G}{8a}\sqrt{\left(c_{11}\frac{s_x}{s}\right)^2 + \left(c_{22}\frac{s_y}{s}\right)^2} \tag{16}$$

where $c_{11} = c_{11}(\sigma, a/b)$ and $c_{22} = c_{22}(\sigma, a/b)$ are the Kalker coefficients [9].

Eventually, the tangential contact force $\underline{T}_c$ has to be calculated. To this aim the creepage $\underline{e}$ can be employed again:

$$\begin{aligned} &T_x = T_c\frac{e_x}{e} \quad T_y = T_c\frac{e_y}{e} \\ &\underline{T}_c = T_x\underline{t}_1 + T_y\underline{t}_2. \end{aligned} \tag{17}$$

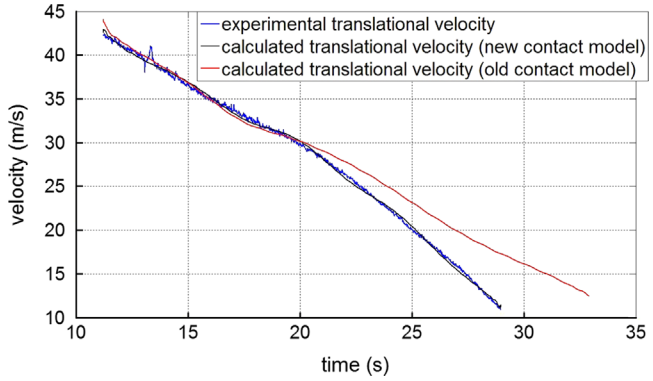

Fig. 16. Experimental velocity v_{w1}^{sp}, the velocity provided by the new model v_{w1}^{new} and the velocity provided by the classic model v_{w1}^{cl} for the I test of group A.

In this phase of the research activity concerning the degraded adhesion, the contact spin at the wheel–rail interface has not been considered. The components of the spin moment $\underline{M}_{sp} = M_{sp}\underline{n}$ produced by the spin creepage $e_{sp} = \underline{\omega}_w \cdot \underline{n}/v_w$ and by the lateral creepage e_y can be neglected because they are quite small. On the other hand the effect of the spin creepage e_{sp} on the lateral contact force T_y may be not negligible. This limitation can be partially overcome thanks to the Polach theory [1,6] that takes into account, in an approximated way, the effect of the spin creepage on the lateral contact force T_{sp}:

$$T_x = T_c\frac{e_x}{e_m} \quad T_y = T_c\frac{e_y}{e_m} + T_{sp}\frac{e_{sp}}{e_m} \tag{18}$$

where e_m is the modulus of the modified translational creepage $\underline{e}_m$ and T_{sp} is the lateral contact force caused by the spin creepage e_{sp}. Both these quantities are calculated in [6] starting from the geometrical and physical characteristics of the system; however T_{sp}, differently form T_c, does not consider the decrease of the adhesion coefficient with increasing creepage and the adhesion recovery under degraded adhesion conditions.

Generally speaking, the role of the contact spin under degraded adhesion conditions, especially in presence of adhesion recovery, is still an open problem.

5.2. Numerical simulations

The vehicle dynamic analysis is focused on the translation and rotational wheel velocities v_{wj}, $r\omega_{wj}$ corresponding to the tests of the tuning group A and the validation group B; more precisely, v_{wj} is the longitudinal component of $\underline{v}_{wj}$, ω_{wj} is the component of $\underline{\omega}_{wj}$ along the wheel rotation axis and, for the sake of simplicity, r is always the nominal wheel radius. These variables have been chosen because they are the most important physical quantities in a braking manoeuvre under degraded adhesion conditions. The variables coming from the 3D multibody model have been compared with the correspondent experimental quantities v_{wj}^{sp}, $r\omega_{wj}^{sp}$ (Section 3).

Firstly, to better highlight the role played by the adhesion recovery in the 3D analysis of the complete vehicle dynamics, the authors report the comparison between the new adhesion model and a classic adhesion model without the adhesion recovery due to the cleaning effect of the friction forces (Fig. 16).

The comparison (performed for the I test of group A) focuses on the translational velocities of vehicle wheels: the experimental velocity v_{w1}^{sp}, the velocity provided by the new model v_{w1}^{new} and the velocity provided by the classic model v_{w1}^{cl}. This simple example well underlines the importance and the effect of the adhesion recovery (caused by the energy dissipation at the contact interface) during the braking of railway vehicles under degraded adhesion conditions.

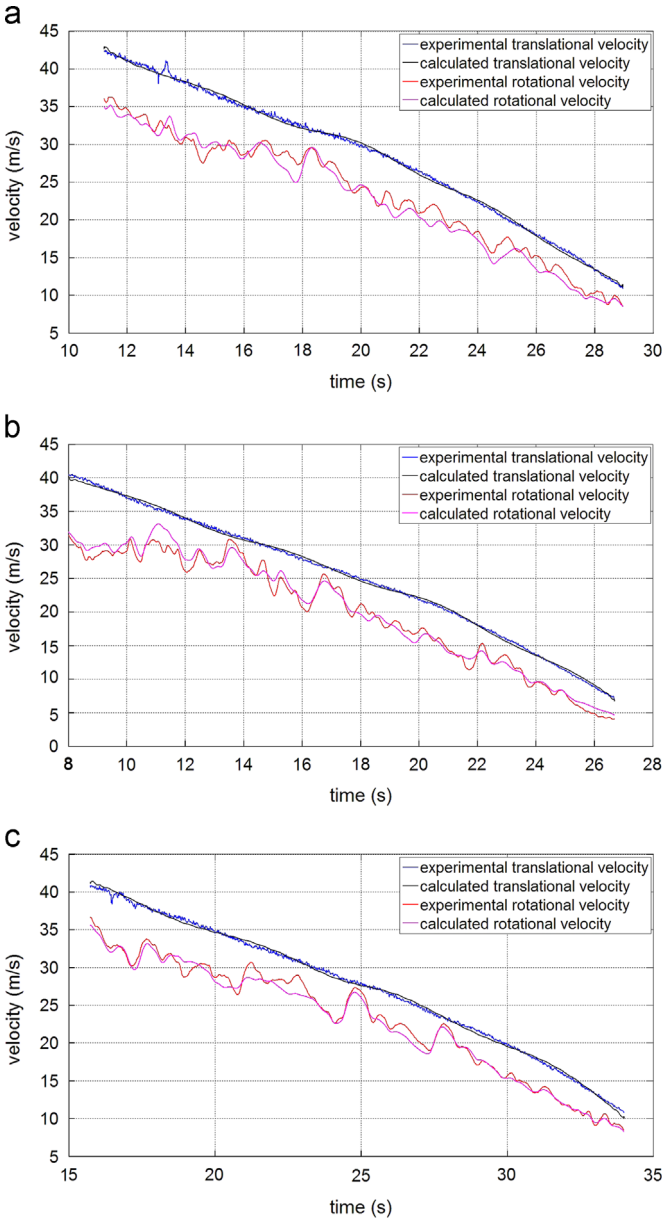

Fig. 17. Translational velocities v_{w1}, v_{w1}^{sp} and rotational velocities $r\omega_{w1}$, $r\omega_{w1}^{sp}$ of the I (a), II (b) and III (c) test of group A.

Secondly, by way of example, the time histories of the translational velocities v_{w1}, v_{w1}^{sp} and the rotational velocities $r\omega_{w1}$, $r\omega_{w1}^{sp}$ are reported in Fig. 17 and 18 for all the three tests of groups A and B.

Additionally, the maximum velocity errors E_j for all the performed tests are considered as well (see Table 7 for E_1):

$$E_j = \max_{t\in[T_I,T_F]}\left|v_{wj}^{sp} - v_{wj}\right|. \tag{19}$$

The results of the analysis show a good agreement in terms of translational velocities v_{wj}, v_{wj}^{sp} especially in the second part of the braking manoeuvre where the adhesion recovery occurs. Concerning the rotational velocities $r\omega_{wj}$, $r\omega_{wj}^{sp}$ (and thus the angular velocities) the correspondence is satisfying. However these physical quantities cannot be locally compared to each other because of the complexity and the chaoticity of the system due, for example, to the presence of discontinuous and threshold elements like the WSP. To better evaluate the behaviour of $r\omega_{wj}$, $r\omega_{wj}^{sp}$ from a global

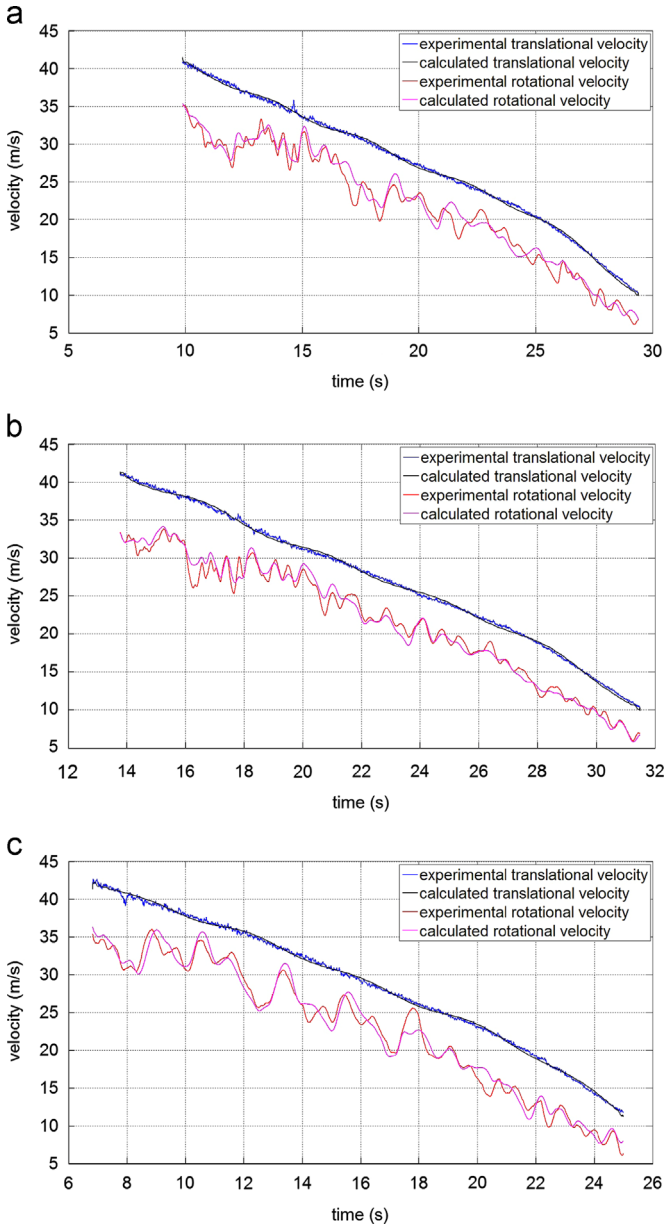

Fig. 18. Translational velocities v_{w1}, v_{w1}^{sp} and rotational velocities $r\omega_{w1}$, $r\omega_{w1}^{sp}$ of the I (a), II (b) and III (c) test of group B.

point of view, it is useful to introduce the statistical means $\bar{s}_j$, $\bar{s}_j^{sp}$ and standard deviations Δ_j, Δ_j^{sp} of the calculated slidings s_j and of the experimental ones s_j^{sp}:

$$\begin{aligned} s_j &= v_{wj} - r\omega_{wj} \\ s_j^{sp} &= v_{wj}^{sp} - r\omega_{wj}^{sp}; \end{aligned} \tag{20}$$

the statistical indices are then evaluated as follows:

$$\begin{aligned} \bar{s}_j &= \frac{1}{T_F - T_I}\int_{T_I}^{T_F} s_j \, dt \\ \bar{s}_j^{sp} &= \frac{1}{T_F - T_I}\int_{T_I}^{T_F} s_j^{sp} \, dt \\ \Delta_j &= \sqrt{\frac{1}{T_F - T_I}\int_{T_I}^{T_F} (s_j - \bar{s}_j)^2 \, dt} \\ \Delta_j^{sp} &= \sqrt{\frac{1}{T_F - T_I}\int_{T_I}^{T_F} (s_j^{sp} - \bar{s}_j^{sp})^2 \, dt} \end{aligned} \tag{21}$$

where T_I and T_F are the initial and final times of the simulation respectively. For instance the means $\bar{s}_1$, $\bar{s}_1^{sp}$ and the standard deviations Δ_1, Δ_1^{sp} of the slidings s_1, s_1^{sp} are summarised in Table 7 for all the three tests of groups A and B and confirm the good matching also in terms of slidings and rotational velocities.

In conclusion, the numerical simulations of the vehicle dynamics during the braking manoeuvre highlight again the capability of the developed model in approximating the complex and highly non-linear behaviour of the degraded adhesion. The result is encouraging especially considering the simplicity of the whole model (only one unknown parameter is involved) and the computational times are very low.

5.3. Computational times

As previously said inside the paper, the new degraded adhesion model is suitable for multibody applications, very important in research areas like the study of the railway vehicle dynamics. In particular high computational performances are required so that the model could be directly implemented online in more general multibody models developed in dedicated environments (in that case Matlab-Simulink).

The data corresponding to the CPU employed in the numerical simulations and the main integration parameters of the ordinary differential equations (ODE) solver are reported in Table 8 [38,31].

To verify the computational efficiency of the degraded adhesion model, the simulation times concerning the whole railway vehicle model (3D multibody model of the vehicle and wheel–rail contact model) have been measured. The computation times reported in Table 9 are referred to the I test of group A and are divided into computation times related to the 3D multibody model and computation times related to the wheel–rail contact model. More specifically four different contact models (always implemented directly online within the 3D multibody model of the vehicle) have been considered. All the contact models share the same contact point detection algorithm and the same solution of the normal problem (the global Hertz theory) while, as regards the tangential contact problem, the following options have been taken into account: the global Kalker theory saturated through the Johnson–Vermeulen formula [9,39], the Kalker FASTSIM algorithm [9], the Polach model [1,6] and the new degraded adhesion model.

Table 7
Maximum velocity errors E_1, sliding means $\bar{s}_1$, $\bar{s}_1^{sp}$ and sliding standard deviations Δ_1, Δ_1^{sp}.

Parameters	Unit	A1	A2	A3	B1	B2	B3
E_1	m/s	2.05	0.90	1.84	1.51	0.91	1.68
$\bar{s}_1^{sp}$	m/s	5.00	5.25	4.23	5.49	5.41	5.83
$\bar{s}_1$	m/s	5.61	4.96	4.61	5.14	5.30	5.73
Δ_1^{sp}	m/s	1.72	2.19	1.59	1.75	1.77	1.78
Δ_1	m/s	1.49	1.79	1.59	1.58	1.45	1.84

Table 8
CPU data and integration parameters.

Parameter	Units	Value
CPU	–	INTEL Xeon E5430 2.66 GHz, 8 GB RAM
Integrator	–	ODE5
Algorithm	–	Dormand-Prince
Order	–	5
Step type	–	Fixed
Step size	s	10^{-4}

Table 9
Computation times of the different wheel rail contact models.

Contact model type	3D Multibody model (s)	Contact model (s)	Whole model (s)
Global Kalker theory	232	118	350
FASTSIM algorithm	235	213	448
Polach Model	232	128	360
New adhesion model	232	130	362

As the numerical results summarised in Table 9 show, the numerical efficiency of the new degraded adhesion model is substantially the same of the other wheel–rail contact models that do not consider degraded adhesion conditions. The achievement of this goal has been possible thanks to the simplicity of the new procedure and allows an easy and efficient online implementability of the adhesion model in more generic multibody models.

6. Conclusions and further developments

In this paper the authors described a model aimed to obtain a better accuracy in reproducing degraded adhesion conditions in vehicle dynamics and railway systems. The followed approach turns out to be suitable for multibody modelling (for instance in Matlab-Simulink and Simpack environments), a very important tool in the considered research areas; furthermore, it assures high computational performances that permit to implement the degraded adhesion model directly online within more general multibody models.

The innovative model focuses on the main phenomena characterising the degraded adhesion: the energy dissipation at the contact interface, the consequent cleaning effect and the resulting adhesion recovery due to the removal of the external unknown contaminants.

Moreover, the simplicity of the followed approach allows the minimisation of the number of the model physical parameters that are very difficult to be experimentally measured; this interesting feature is fundamental because most of the physical characteristics of the contaminants are totally unknown in practice.

The new adhesion model has been validated through experimental data provided by Trenitalia S.p.A. and coming from on-track tests carried out in Velim (Czech Republic) on a straight railway track characterised by degraded adhesion conditions. The tests have been performed with the railway vehicle UIC-Z1 equipped with a fully-working Wheel Slide Protection (WSP) system.

Concerning the future developments, firstly further experimental tests will be performed by Trenitalia, regarding both braking and traction phases. The new experimental data will allow a better tuning of the model geometrical and physical parameters.

Concerning this topic, particular attention will be paid to the model sensitivity against uncertainties affecting inertia, suspension and contact parameters. Furthermore, the effect of different friction modifiers and of different contaminant deployment techniques will be taken into account.

Secondly, many model improvements will be considered. More particularly, new theoretical and experimental relations among the adhesion coefficient f, the specific dissipated energy W_{sp} and the limit adhesion levels f_d, f_r (degraded adhesion and adhesion recovery) will be introduced and analysed. The new relations will also have to consider the differences in terms of adhesion coefficient between the wheels of the same train; in fact the cleaning effect due to the action of the first wheels guarantees better adhesion conditions to the following wheels.

At the same time the role of the spin at the contact interface will be investigated to try to include the spin effect into the degraded adhesion model.

In addition, to improve the estimation of the normal contact forces (see Section 3.2), a more accurate dynamical measure of the wheel weight (performed online during the new experimental tests) will be carried out.

Finally, the new degraded adhesion model will be implemented within different 3D multibody models of railway vehicles (developed in dedicated environments like Matlab-Simulink, Simpack, etc.) operating on generic curvilinear railway tracks. During this phase different contact and degraded adhesion models will be tested, with and without adhesion recovery (due to the cleaning effect of the friction contact forces). This way, the effect of the adhesion recovery on the railway vehicle dynamics, the wheel–rail contact and the wear affecting the wheel and rail surfaces will be better investigated.

Acknowledgements

The authors would like to thank the Trenitalia archives for supplying the experimental data relative to the braking tests under degraded adhesion conditions.

References

[1] Polach O. Creep forces in simulations of traction vehicles running on adhesion limit. Wear 2005;258:992–1000.
[2] Meli E, Falomi S, Malvezzi M, Rindi A. Determination of wheel–rail contact points with semianalytic methods. Multibody System Dynamics 2008;20:327–58.
[3] Pombo J, Ambrosio J. Application of a wheel–rail contact model to railway dynamics in small radius curved tracks. Multibody System Dynamics 2008;19:91–114.
[4] Pombo J, Silva AJ. A new wheel–rail contact model for railway dynamics. Vehicle System Dynamics 2007;45:165–89.
[5] Iwnicki S. Simulation of wheel–rail contact forces. Fatigue and Fracture of Engineering Materials and Structures 2003;26:887–900.
[6] Polach O. A fast wheelrail forces calculation computer code. Vehicle System Dynamics 1999;33:728–39.
[7] Falomi S, Malvezzi M, Meli E. Multibody modeling of railway vehicles: innovative algorithms for the detection of wheel–rail contact points. Wear 2011;271:453–61.
[8] Magheri S, Malvezzi M, Meli E, Rindi A. An innovative wheel–rail contact model for multibody applications. Wear 2011;271:462–71.
[9] Kalker J. Three-Dimensional Elastic Bodies in Rolling Contact. Norwell, MA: Kluwer Academic Publishers; 1990.
[10] Zhu Y, Olofsson U, Soederberg A. Adhesion modeling in the wheel–rail contact under dry and lubricated conditions using measured 3d surfaces. Tribology International 2013;61:1–10.
[11] Egana J, Vinolas J, Gil-Negrete N. Effect of liquid high positive friction (hpf) modifier on wheel–rail contact and rail corrugation. Tribology International 2005;38:769–74.
[12] Arias-Cuevas O, Li Z, Lewis R. Investigating the lubricity and electrical insulation caused by sanding in dry wheel–rail contacts. Tribology Letters 2010;37:623–35.
[13] Li Z, Arias-Cuevas O, Lewis R, Gallardo-Hernndez EA. Rolling–sliding laboratory tests of friction modifiers in leaf contaminated wheelrail contacts. Tribology Letters 2009;33:97–109.
[14] Cann PM. The leaves on the line problem—a study of leaf residue film formation and lubricity under laboratory test conditions. Tribology Letters 2006;24:151–8.
[15] Arias-Cuevas O, Li Z, Lewis R. A laboratory investigation on the influence of the particle size and slip during sanding on the adhesion and wear in the wheel–rail contact. Wear 2011;271:14–24.
[16] Arias-Cuevas O, Li Z, Lewis R, Gallardo-Hernandez EA. Rollingsliding laboratory tests of friction modifiers in dry and wet wheel–rail contacts. Wear 2010;268:543–51.
[17] Wang WJ, Zhang HF, Wang HY, Liu QY, Zhu MH. Study on the adhesion behavior of wheel/rail under oil, water and sanding conditions. Wear 2011;271:2693–8.
[18] Niccolini E, Berthier Y. Wheel–rail adhesion: laboratory study of natural third body role on locomotives wheels and rails. Wear 2005;258:1172–8.
[19] Gallardo-Hernandez E, Lewis R. Twin disc assessment of wheel/rail adhesion. Wear 2008;265:1309–16.

[20] Eadie D, Kalousek J, Chiddick K. The role of high positive friction (hpf) modifier in the control of short pitch corrugations and related phenomena. Wear 2002;253:185–92.
[21] Descartes S, Desrayaud C, Niccolini E, Berthier Y. Presence and role of the third body in a wheel–rail contact. Wear 2005;258:1081–90.
[22] Chen H, Ban T, Ishida M, Nakahara T. Experimental investigation of influential factors on adhesion between wheel and rail under wet conditions. Wear 2008;265:1504–11.
[23] M. Boiteux, Le probleme de l'adherence en freinage. Revue generale des chemins de fer (1986) 59–72.
[24] Zhang W, Chen J, Wu X, Jin X. Wheel/rail adhesion and analysis by using full scale roller rig. Wear 2002;253:82–8.
[25] Blau PJ. Embedding wear models into friction models. Tribology Letters 2009;34:75–9.
[26] Voltr, P, Lata, M, Cerny, O, Measuring of wheel–rail adhesion characteristics at a test stand. In: Proceedings of XVIII internation conference on engineering mechanics. Czech Republic; 2012.
[27] Conti E, Meli B, Pugi L, Malvezzi M, Bartolini F, Allotta A, et al. A numerical model of a HIL scaled roller rig for simulation of wheel–rail degraded adhesion condition. Vehicle System Dynamics 2012;50:775–804.
[28] Allotta B, Malvezzi M, Pugi L, Ridolfi A, Rindi A, Vettori G. Evaluation of odometry algorithm performances using a railway vehicle dynamic model. Vehicle System Dynamics 2012;50:699–724.
[29] Allotta, B., Conti, R., Malvezzi, M., Meli, E., Pugi, L., Ridolfi, A., Numerical simulation of a HIL full scale roller–rig model to reproduce degraded adhesion conditions in railway applications. iIn:n: European congress on computational methods in applied sciences and engineering (ECCOMAS 2012). Austria; 2012.
[30] Malvezzi, M., Pugi, L., Ridolfi, A., Cangioli, F., Rindi, A., Three dimensional modelling of wheel–rail degraded adhesion conditions. In: Proceedings of IAVSD 2011. Manchester; 2011.
[31] www.mathworks.com, Official Site of Mathworks, Natick, MA, USA, 2012.
[32] www.simpack.com, Official Site of Simpack GmbH, Gilching, Germany, 2012.
[33] Trenitalia SpA, UIC-Z1 coach. Internal report of Trenitalia. Rome, Italy. 2000.
[34] Trenitalia SpA, WSP systems. Internal report of Trenitalia. Rome, Italy; 2006.
[35] Trenitalia SpA, On-track braking tests. Internal report of Trenitalia. Rome, Italy; 2005.
[36] Kelley C. Iterative Methods for Linear and Nonlinear Equations. Philadelphia PA, USA: SIAM; 1995.
[37] Nocedal J, Wright S. Numerical Optimisation. Berlin, Germany: Springer Series in Operation Research; 1999.
[38] Shampine L, Reichelt M. The matlab ode suite. SIAM Journal of Scientific Computation 1997;18:1–22.
[39] Dukkipati R, Amyot J. Computer Aided Simulation in Railway Dynamics. New York, USA: Dekker; 1988.
[40] Railway applications, braking, wheel slide protection. UNI EN 15595, May, 2009.
[41] Allotta B, Conti R, Meli E, Pugi L, Ridolfi A. Development of a HIL railway roller–rig model for the traction and braking testing activities under degraded adhesion conditions. International Journal of Non-Linear Mechanics 2013;57:50–64.